

Topologically protected braiding in a single wire using Floquet Majorana modes

Bela Bauer,¹ T. Pereg-Barnea,^{2,3} Torsten Karzig,¹ Maria-Theresa Rieder,³ Gil Refael,^{4,5} Erez Berg,^{3,6} and Yuval Oreg³

¹Station Q, Microsoft Corporation, Santa Barbara, California 93106 USA

²Department of Physics, McGill University, Montréal, Québec, Canada

³Department of Condensed Matter Physics, Weizmann Institute of Science, Rehovot 76100, Israel

⁴Walter Burke Institute for Theoretical Physics and Institute for Quantum Information and Matter, California Institute of Technology, Pasadena, California 91125 USA

⁵Department of Physics, California Institute of Technology, Pasadena, California 91125 USA

⁶Department of Physics, James Franck Institute, University of Chicago, Chicago, Illinois 60637 USA

(Dated: October 10, 2018)

Majorana zero modes are a promising platform for topologically protected quantum information processing. Their non-Abelian nature, which is key for performing quantum gates, is most prominently exhibited through braiding. While originally formulated for two-dimensional (2d) systems, it has been shown that braiding can also be realized using one-dimensional (1d) wires by forming an essentially two-dimensional network. Here, we show that in driven systems far from equilibrium, one can do away with the second spatial dimension altogether by instead using quasienergy as the second dimension. To realize this, we use a Floquet topological superconductor which can exhibit Majorana modes at two special eigenvalues of the evolution operator, 0 and π , and thus can realize four Majorana modes in a single, driven quantum wire. We describe and numerically evaluate a protocol that realizes a topologically protected exchange of two Majorana zero modes in a single wire by adiabatically modulating the Floquet drive and using the π modes as auxiliary degrees of freedom.

Non-equilibrium systems have recently been shown to host a variety of novel phenomena with no equilibrium system equivalent. One of the early examples was discussed in Ref. 1, which demonstrated that a driven p -wave superconducting wire can possess not only the well-known Majorana zero modes (MZMs) at zero energy [2, 3], but also so-called Majorana π modes (MPMs) at frequency $\omega/2$, with ω the frequency of the external drive. These are but an example of a broader class of anomalous Floquet topological phases [4, 5], with no analogue in static (time-independent) systems. Other examples include Floquet symmetry-protected topological (Floquet-SPT) phases [6–9], and the closely related time-crystals [10–15], where periodically driven interacting and disordered systems show a response at a multiple of the drive period. In all these systems, discrete time-translation symmetry protects novel quantum states.

It is natural to ask whether the topological degrees of freedom that emerge in driven systems can be used to supplement equilibrium topological phases. Particularly interesting are Majorana zero modes [16–20]. It is well-known that they exhibit non-Abelian statistics: When several MZMs are present, the many-body ground state becomes degenerate, and adiabatically exchanging two well-separated MZMs carries out a non-trivial unitary transformation within the ground state manifold [21, 22]. Such braiding operations form the basis of topological quantum computation [23, 24]. Physically, MZMs are realized as zero-energy excitations in one- [2, 25–28] and two- [29–32] dimensional topological superconductors. While these systems are of great interest for quantum

computing, non-Abelian braiding itself remains a tantalizing fundamental effect, and demonstrating it would be a tremendous breakthrough.

In the following, we show that MPMs emerging in driven systems allow for remarkable new braiding protocols, going beyond what is possible in equilibrium systems. Strictly speaking, braiding is only possible beyond one spatial dimension: two quasi-particles cannot be exchanged on a single wire while being distant from each other. In this work, however, we show that in periodically driven systems, *quasienergy* provides an additional synthetic dimension that can be used in conjunction with real space. Roughly speaking, the two kinds of Majorana states in Floquet superconductors – MZMs and MPMs – live a parallel existence at two different frequencies. As pointed out first in Ref. [1], they are precisely decoupled from each other as long as the drive is invariant under time-translation by one period. It follows that half-frequency pulses can be used to couple the MZMs and MPMs [33].

Refs. [34, 35] also propose using a combination of MZMs and MPMs as well as half-frequency pulses to simulate braiding operations. However, the scheme we perform here is a *non-local* braid rather than a local operation at one end of the system. The non-locality of our scheme leads to topological protection against local perturbations.

Floquet braiding—We begin with a 1d topological superconductor, which under a period- T drive may enter a Floquet topological superconducting phase [1, 36]. As a function of material and drive parameters, each edge of

the system may have no MZMs, one MZM and/or another Majorana mode with energy at the Floquet zone boundary. We denote this quasienergy by π/T and refer to the corresponding Majorana mode as a Majorana π mode (MPM). A time-periodic system only allows quasienergies inside the Floquet zone, $-\pi/T \leq \epsilon < \pi/T$. Therefore, particle-hole symmetry requires that Majorana modes come in pairs at all energies except zero and π/T , which is where unpaired Majorana modes can be found. Moreover, as long as time periodicity is conserved, the MZMs and MPMs do not hybridize even if their wavefunctions overlap in space. This property allows us to move them past each other and enables the procedure, which does not require any fine-tuning of the Hamiltonian or its time dependence [37].

There are several experimental schemes for MZM exchange. The simplest one is to physically move the MZMs [38]. Alternatively, consider a system made up of four MZMs at fixed locations, but with tunable interactions between them [39–42]; in this case, at any time during the braid two of the four Majorana modes are strongly coupled, but the dominant coupling is changed in a particular order to effectively perform a braid operation. Similarly, a sequence of 2-MZM measurements can be used to implement measurement-only variants of braiding [43–45]. In either case, at least two quantum wires are required.

Our proposed braiding protocol is most closely akin to an approach with four MZMs, of which two are coupled at any time. Our four states, however, are a pair of MZMs and another pair of MPMs. To introduce interactions between MZMs and MPMs, we apply a time-dependent perturbation in restricted regions, thus locally breaking the time-translation symmetry that protects the MPMs. We numerically confirm below that such a perturbation acts only locally even though time-translation symmetry is a global symmetry. We then combine this with moving the MZMs and MPMs to achieve braiding.

Two-part drive model—Let us consider the Kitaev Hamiltonian:

$$H(\mu_i, w_i, \Delta_i) = \sum_i \left[-\mu_i c_i^\dagger c_i - \frac{w_i}{2} (c_i^\dagger c_{i+1} + \text{h.c.}) \right] + \sum_i \frac{\Delta_i}{2} (c_i c_{i+1} + \text{h.c.}) \quad (1)$$

and construct the Floquet operator with period T

$$U_F = e^{-iH_0 T/2} e^{-iH_1 T/2} \quad (2)$$

$$H_0 = H(\mu_i = 0, w_i = 2\pi\lambda_0/T, \Delta_i = -2\pi\lambda_0/T) \quad (3)$$

$$H_1 = H(\mu_i = 2\pi\lambda_1/T, w_i = 0, \Delta_i = 0), \quad (4)$$

where H_0 is the Hamiltonian of a Kitaev chain at the ‘sweet spot’ of the topological phase (see below) and H_1 is the Hamiltonian of a trivial phase with only chemical potential. For couplings $\lambda_0, \lambda_1 \in [0, 1]$ ($\hbar = 1$ throughout), this gives rise to the phase diagram [12] (Fig. 1)

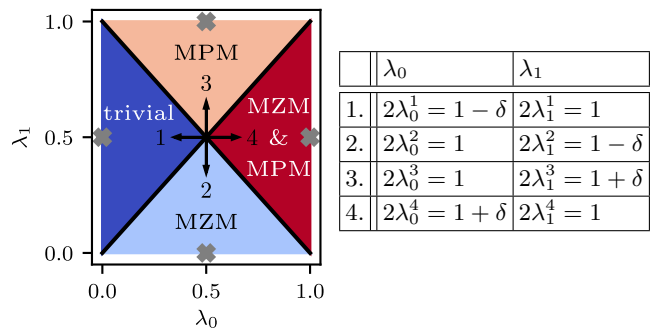


FIG. 1. *Left*: Phase diagram of the Floquet system in terms of the strength of the topological (trivial) Hamiltonian $H_0(H_1)$ in the two-part drive, see Eqs. (3),(4). It is possible to realize 4 phases characterized by the presence of zero or π modes: 1) trivial 2) MZMs 3) MPMs 4) MZMs and MPMs. The gray crosses mark the sweet spots of the corresponding phases with vanishing correlation lengths. *Right*: Parameterization used in Eq. (2) to obtain the phase diagram. The parameter δ quantifies the distance to the critical point and the direction of increasing δ is indicated in the left panel.

with the four phases characterized by the presence or absence of MZMs and MPMs. Each phase contains a point of vanishing correlation length, *aka* ‘sweet spots,’ where the MZM and/or MPM states are localized on a single site. The sweet spots are indicated by the gray crosses in Fig. 1. These points are discussed in the Supplemental Material. A convenient choice of parameters is given by that of the right panel of Fig. 1, where the superscript refers to the phases as follows: 1–trivial phase, 2–MZM only, 3–MPM only, and 4–both MZMs and MPMs. The parameter δ quantifies the distance of all the phases to the critical point and is connected to the correlation length, with $\delta = 0$ corresponding to the critical point and $\delta = 1$ to the points with vanishing correlation length (the black arrows in the left panel of Fig. 1 indicate the direction of increasing δ). Throughout, we consider U_F to encode an elementary Floquet cycle with period T .

To implement the Floquet braiding protocol, consider an inhomogeneous systems, where different regions are in different phases with the possibility to move phase boundaries. Let \vec{p} be a vector whose elements $p_i \in \{1, 2, 3, 4\}$ indicate that the parameters of the bond i correspond to phase p_i . We can then generalize the Floquet drive of Eq. (2) to the inhomogeneous case:

$$U_F(\vec{p}) = e^{-iH_0(\vec{p})T/2} e^{-iH_1(\vec{p})T/2} \quad (5)$$

$$H_0(\vec{p}) = H(\mu_i = 0, w_i = 2\pi\lambda_0^{p_i}/T, \Delta_i = -2\pi\lambda_0^{p_i}/T) \quad (6)$$

$$H_1(\vec{p}) = H(\mu_i = 2\pi\lambda_1^{p_i}/T, w_i = 0, \Delta_i = 0). \quad (7)$$

In an inhomogeneous system, MZMs and MPMs also form at the interfaces between phases with different topological order. For example, half of the system could be in phase 2 (MZM), and the other half in phase 4 (MZM and MPM). In such a case, the MZMs will form at the end of the system, one MPM will form at one end of the

system, and the other one in the middle of the system.

To move the spatial phase boundaries as a function of time, we interpolate between two different systems described by vectors \vec{p} and \vec{q} by continuously tuning a parameter $s \in [0, 1]$ and applying Floquet drives analogous to Eq. (5), but with $H_0 = (1 - f(s))H_0(\vec{p}) + f(s)H_0(\vec{q})$, and similarly for H_1 . Here, $f(s)$ is a function with $f(0) = 0$ and $f(1) = 1$; in our simulations, we choose $f(s) = \sin(s\pi/2)^2$. We evolve from $s = 0$ to $s = 1$ over N_s time steps. For sufficiently large N_s , if the initial state of this operation is an eigenstate of $U_F(\vec{p})$, the final state will be an eigenstate of $U_F(\vec{q})$. This can be considered a version of adiabaticity for driven systems [46–48] and be understood by the formal relation between each U_F to a Floquet Hamiltonian $H_F = i(\log U_F)/T$. The spectrum of H_F corresponds to the quasi-energy spectrum of the Floquet unitary. We can therefore relate the deformation from $U_F(\vec{p})$ to $U_F(\vec{q})$ to a deformation of the corresponding Floquet Hamiltonian from $H_F(\vec{p})$ to $H_F(\vec{q})$. The adiabatic condition can then be formulated with respect to the quasienergy spectrum of H_F . Dynamically changing the Floquet operator weakly breaks the time-translation symmetry that protects the MPMs similar to how energy conservation is broken in time-dependent equilibrium systems. To reduce the corresponding errors in the braiding protocol, we choose a smooth evolution which strongly suppresses the π/T components as N_s becomes large except for the desired local perturbations discussed below.

Local time-translation symmetry breaking—As a final ingredient to our protocol, we need to be able to couple nearby MZMs and MPMs. To explicitly introduce such a coupling, we insert an operator U_{pert} after every two elementary Floquet cycles, thus changing U_F^n to $(U_F^2 U_{\text{pert}})^{n/2}$. The coupling can be understood by considering that eigenvectors corresponding to quasi energies 0 and π/T in U_F all correspond to quasienergy 0 in U_F^2 , and are therefore susceptible to perturbations. Importantly, if U_{pert} acts only in a specific region of the system, it will only couple a pair of nearby MZMs and MPMs in that region while leaving the ones far away unperturbed.

To confirm this picture, we turn to numerical simulations, which we perform using established techniques [49]. We compute the spectrum of the operator $U_F(\delta)^2 U_{\text{pert}}$, where $U_F(\delta)$ is the Floquet operator of Eq. (2) with the parameters chosen inside phase 4 which exhibits both zero and π modes, and U_{pert} acting only on one half of the system. Specifically, we choose

$$U_{\text{pert}}(\lambda_{\text{pert}}) = e^{iT H(T\mu_i = \lambda_{\text{pert}}, Tw_i = \lambda_{\text{pert}}, T\Delta_i = -\lambda_{\text{pert}})}, \quad (8)$$

where μ_i , w_i and Δ_i are non-vanishing only in the right half of the system. For $\lambda_{\text{pert}} = 0$, time-translation symmetry for a single Floquet cycle is restored and the system will exhibit two localized and uncoupled modes at each end. However, when $\lambda_{\text{pert}} > 0$, the (0 and π) modes

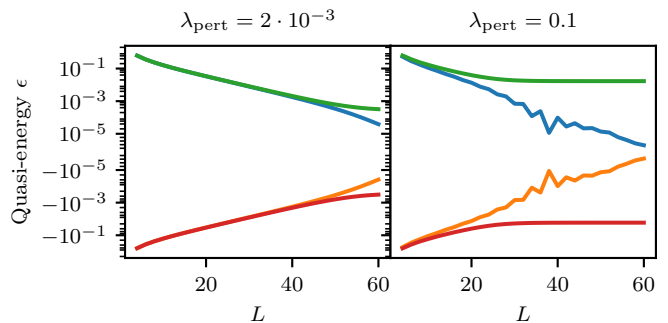


FIG. 2. Quasi energies closest to zero for Floquet evolutions over two cycles for a system of length L in phase 4 ($\delta = 0.09$) for different strengths of time-translational symmetry breaking perturbations applied the right end of the system. Left, right panel show the case of a very weak ($\lambda_{\text{pert}} = 2 \cdot 10^{-3}$) and moderate perturbation ($\lambda_{\text{pert}} = 0.1$), respectively. In the unperturbed case, each level is two-fold degenerate corresponding to two MZMs and two MPMs. In the perturbed case, since the pair of MZM and MPM at the right end of the system is split, only the MZM and MPM at the left end remains. Notice that when $\lambda_{\text{pert}} \neq 0$ the period is doubled, and as a result the MZMs and MPMs both get folded to the vicinity of $\epsilon = 0$.

at the right end split, while the MZM and MPM at the left remain as the only unsplit modes. This behavior is reflected in the spectrum shown in Fig. 2, which shows the lowest (in absolute value) quasi-energies of $U_F(\delta)^2 U_{\text{pert}}$ for two choices of λ_{pert} . Due to particle-hole symmetry, the positive and negative quasi energies mirror each other. For the unperturbed case, $\lambda_{\text{pert}} = 0$, we find that four eigenvalues approach zero exponentially as the system size is increased. Upon perturbing the system, two of them saturate to a value of order λ_{pert} , while the others continue to decrease exponentially with the same exponent that governed the unperturbed case.

Braiding protocol—We now turn to the full braid protocol. We start and end in a configuration where the entire system is in the regular, undriven, Kitaev phase, exhibiting MZMs at the system’s edge. This allows state preparation in an undriven system. We then turn on the Floquet drive to perform a braid operation by following the steps in Fig. 3. Since all the Floquet-drive phases (2) are gapped around the respective 0 or π modes, and the protocol never drives extended regions of the system through the phase transition at once, the Floquet quasienergy spectrum at each step of the evolution remains gapped. Therefore adiabaticity is maintained even in the thermodynamic limit by choosing N_s which interpolates the move of the phase boundary by one site sufficiently large.

Throughout the evolution, the system contains at least a pair of MZMs, and, at intermediate stages, an additional pair of MPMs. In the case where both MZMs and MPMs and hence a total of four modes are present,

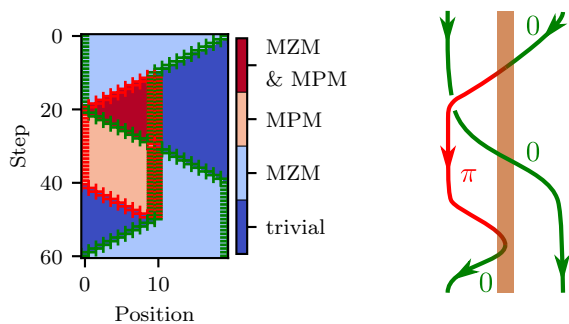


FIG. 3. *Left*: Full braid protocol for a system of $L = 20$ sites. The colors correspond to different phases; green (red) crosses indicate the locations of MZMs (MPMs). *Right*: Schematic representation of the braiding process of two MZMs. In the center region it is possible to convert between MZMs (denoted by 0) MPMs (denoted by π). After the right MZM has been converted into a MPM it can be safely moved past the left MZM in the region where time-translational symmetry is preserved.

we need to fix which pair encodes the quantum information. To achieve this, we apply a local time-translation-symmetry-breaking perturbation in a region in the middle of the system. Therefore, when both an MZM and an MPM are in the middle, they are split to finite energy and only two low-energy modes remain, which thus carry the encoded quantum state. When three modes, e.g. two MPMs and an MZM, are in the perturbed regime, one mode (which is a linear combination of the three modes) remains unperturbed while two are split away to finite energy. This enables us to effectively convert a MZM to a MPM mode and vice versa as indicated in Fig. 3.

A subtle point arises if both a perturbation that breaks time-translation symmetry is present, and the Floquet drive is slowly changed to move phase boundaries as described above. In that case the Floquet unitary of a single cycle is $U_F(s)$ with s a slowly changing parameter such that consecutive cycles are described by $U_F(s')U_F(s)$ with $s' - s = 1/N_s$. When adding a perturbation U_{pert} to this, it is important that the parameter s is still changed in every step, i.e. the perturbed evolution over two cycles is $U_{\text{pert}}U_F(s')U_F(s)$. The perturbation will still be effective as long as $U_F(s)$ and $U_F(s')$ are sufficiently close. While it may appear more natural to change the parameter s only every two cycles when inserting the perturbation, this inadvertently induces an additional half-frequency perturbation. While the strength of this accidental perturbation vanishes in the adiabatic limit $N_s \rightarrow \infty$ where s is changed only infinitesimally, it is also applied a diverging number of times in that limit, and thus a net effect remains. The protocol then exhibits non-universal corrections even when performed in the adiabatic limit. Similar corrections may be explicitly exploited to perform certain geometric quantum gates [34, 35].

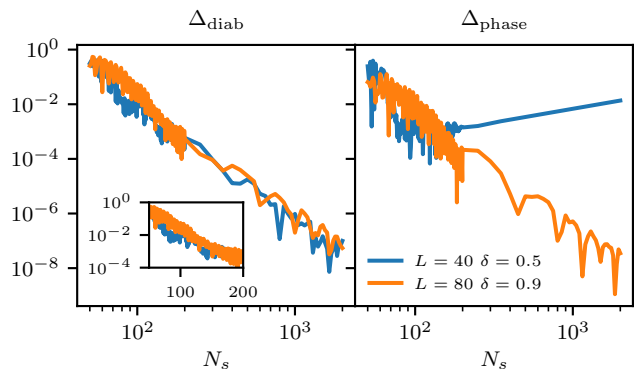


FIG. 4. Errors in the braid protocol, measured by the deviation from unitarity of the evolution in the low-energy subspace (left panel) and deviation in the applied phase (right panel, see main text for definitions of Δ_{diab} and Δ_{phase}) as a function of the number of interpolation steps between stages of the protocol. In the limit of $N_s \rightarrow \infty$, adiabaticity is recovered. The errors generally vanish with a lower-law, however for fast protocols ($N_s < 200$) an exponential transient behavior is observed. In the phase error, the dependence on N_s is non-monotonic: for sufficiently slow protocols, the evolution becomes adiabatic with respect to the residual finite-size splitting of Majorana modes. Parameters used are $\lambda_{\text{pert}} = 0.2$.

Numerical results—A numerical implementation of the dynamical braiding is summarized in Fig. 4. Since the Hamiltonian is quadratic, the evolution of operators of the form $\vec{v} \cdot \vec{\gamma}$, where $\vec{\gamma}$ is a vector of Majorana operators such that $2c_i = \gamma_{2i-1} + i\gamma_{2i}$, can be represented by an orthogonal matrix \bar{U} . Over the entire process, $\vec{v} \cdot \vec{\gamma}$ evolves into $(\bar{U}\vec{v}) \cdot \vec{\gamma}$ (see Supplementary Information for details).

To define the relevant error measures, let $\gamma_{1,2} = \vec{v}_{1,2} \cdot \vec{\gamma}$ be initial (and final) MZMs. Then, we compute the 2×2 matrix $(U_r)_{\alpha,\beta} = \vec{v}_\alpha^T \bar{U} \vec{v}_\beta$ ($\alpha, \beta = 1, 2$), which encapsulates how the entire time evolution acts on the low-energy Majorana subspace. In the ideal limit, $U_r = i\sigma^y$, where σ^y denotes the usual Pauli matrix. We quantify deviations from this using two measures: $\Delta_{\text{diab}} = |U_r^\dagger U_r - 1|$ captures deviations from unitarity, in particular diabatic corrections that excite fermions from the low-energy subspace to the excited states. Secondly, we compute the two eigenvalues of U_r as $(r_1 e^{i\phi_1}, r_2 e^{i\phi_2})$. In the ideal case, we expect $r_1 = r_2 = 1$ and $\phi_1 = -\pi/2$, $\phi_2 = \pi/2$. We define deviations from this as $\Delta_{\text{phase}} = |\phi_1 + \pi/2| + |\phi_2 - \pi/2|$, where we sort eigenvalues such that $\phi_1 \geq \phi_2$. Both measures are chosen to be independent of the basis choice for the Majorana subspace since it is not unique in the case when they are exactly degenerate.

Fig. 4 shows that increasing N_s to perform a slower protocol improves the errors. At short times, the accuracy improves exponentially, while at long times a power-law behavior is observed, consistent with the non-analytic time-dependence of the driving Hamiltonian. Interestingly, the two error measures can exhibit qualita-

tively different behavior, as shown in the long-time behavior for $L = 40$, $\delta = 0.5$: while the diabatic corrections continue to decrease, the error in the applied phase reaches a minimum value beyond which it increases again. This occurs because very slow protocols resolve the splitting of the low-energy manifold. For larger system sizes, such as $L = 80$ and $\delta = 0.9$, this crossover would occur at much slower protocol times (larger N_s). In most relevant parameter regimes, the error is dominated by diabatic corrections and not finite-size corrections, i.e. the error is independent of system size for all but the smallest systems. Details of the dependence of Δ_{diab} on other parameters such as δ and λ_{pert} can be found in the Supplemental Material.

Topological protection & Outlook—To conclude, we discuss in what sense braiding as described here is topologically protected. Just as many other new phenomena in periodically driven systems, MPMs are protected by time-translation symmetry. Therefore, braiding of MPMs is topologically protected only if no processes that break the periodicity of the drive are present. A subtle issue is that the braid process itself breaks time-translation symmetry and thus gives rise to dynamical corrections, but as we have shown above these can be systematically suppressed by adiabatically changing the drive parameters. Similar diabatic errors may also occur in the braiding of MZMs if operations are performed away from the adiabatic limit [50–61].

Importantly, unlike other symmetries that can give rise to multiple MZMs in a single wire, our Floquet approach does not require careful tuning of the instantaneous Hamiltonian. Thus it is much more experimentally accessible. We provide a perspective towards such realizations in systems based on superconducting quantum dot chains [62–64] in the Supplemental Material, where in particular we discuss a model that is able to implement the same behavior but requires time-dependent control of only a single parameter. Perhaps the simplest realization, however, would be using a quantum wire proximity coupled to two superconductors, one grounded, and the other at a finite voltage. The AC Josephson effect gives rise to the time dependence leading to MPM's [65].

An important caveat is that we relied on the absence of heating. While this assumption is appropriate for the non-interacting limit, it is well-known that driven interacting systems generically heat to infinite temperature [66–68]. However, there are known mechanisms such as many-body localization [68–71] as well as the pre-thermalization [72–79] which can be used to avoid heating and stabilize the results discussed here. The details of this interacting scenario are an open question left to future work.

This work was supported by NSERC DG (TPB), the BSF and ISF grants and by the European Research Council under the European Communitys Seventh Framework Program (FP7/20072013)/ERC - Grant

agreement MUNATOP-340210. YO and EB acknowledge support from CRC 183 of the Deutsche Forschungsgemeinschaft. We are also grateful for the hospitality of the Aspen Center for Physics, which is supported by National Science Foundation grant PHY-1607761, and where part of the work was done.

-
- [1] L. Jiang, T. Kitagawa, J. Alicea, A. R. Akhmerov, D. Pekker, G. Refael, J. I. Cirac, E. Demler, M. D. Lukin, and P. Zoller, *Phys. Rev. Lett.* **106**, 220402 (2011).
 - [2] A. Kitaev, *Phys. Usp.* **44**, 131 (2001).
 - [3] O. Motrunich, K. Damle, and D. A. Huse, *Phys. Rev. B* **63**, 224204 (2001).
 - [4] T. Kitagawa, E. Berg, M. Rudner, and E. Demler, *Phys. Rev. B* **82**, 235114 (2010).
 - [5] M. S. Rudner, N. H. Lindner, E. Berg, and M. Levin, *Phys. Rev. X* **3**, 031005 (2013).
 - [6] C. W. von Keyserlingk and S. L. Sondhi, *Phys. Rev. B* **93**, 245145 (2016), arXiv:1602.02157.
 - [7] D. V. Else and C. Nayak, “Classification of topological phases in periodically driven interacting systems,” (2016), arXiv:1602.04804.
 - [8] A. C. Potter, T. Morimoto, and A. Vishwanath, *Phys. Rev. X* **6**, 041001, arXiv:1602.05194.
 - [9] R. Roy and F. Harper, *Phys. Rev. B* **94**, 125105, arXiv:1602.08089.
 - [10] F. Wilczek, *Phys. Rev. Lett.* **109**, 160401 (2012), arXiv:1202.2539 [quant-ph].
 - [11] A. Shapere and F. Wilczek, *Phys. Rev. Lett.* **109**, 160402 (2012), arXiv:1202.2537 [cond-mat.other].
 - [12] V. Khemani, A. Lazarides, R. Moessner, and S. L. Sondhi, *Phys. Rev. Lett.* **116**, 250401 (2016).
 - [13] D. V. Else, B. Bauer, and C. Nayak, *Phys. Rev. Lett.* **117**, 090402 (2016).
 - [14] A. C. Potter, T. Morimoto, and A. Vishwanath, *Phys. Rev. X* **6**, 041001 (2016).
 - [15] C. W. von Keyserlingk, V. Khemani, and S. L. Sondhi, *Phys. Rev. B* **94**, 085112 (2016), arXiv:1605.00639.
 - [16] J. Alicea, *Rep. Prog. Phys.* **75**, 076501 (2012).
 - [17] C. Beenakker, *Annu. Rev. Condens. Matter Phys.* **4**, 113 (2013).
 - [18] S. D. Sarma, M. Freedman, and C. Nayak, *NPJ Quant. Inf.* **1**, 15001 (2015).
 - [19] R. M. Lutchyn, E. P. a. M. Bakkers, L. P. Kouwenhoven, P. Krogstrup, C. M. Marcus, and Y. Oreg, *Nat. Rev. Mater.* **3**, 52 (2018), arXiv:1707.04899.
 - [20] R. Aguado, *Riv. Nuovo Cimento* **40**, 523 (2017), arXiv:1711.00011.
 - [21] D. A. Ivanov, *Physical Review Letters* **86**, 268 (2001), cond-mat/0005069.
 - [22] A. Stern, F. von Oppen, and E. Mariantoni, *Phys. Rev. B* **70**, 205338 (2004), cond-mat/0310273.
 - [23] A. Y. Kitaev, *Annals of Physics* **303**, 2 (2003), quant-ph/9707021.
 - [24] C. Nayak, S. H. Simon, A. Stern, M. Freedman, and S. Das Sarma, *Reviews of Modern Physics* **80**, 1083 (2008), arXiv:0707.1889 [cond-mat.str-el].
 - [25] R. M. Lutchyn, J. D. Sau, and S. Das Sarma, *Physical Review Letters* **105**, 077001 (2010), arXiv:1002.4033 [cond-mat.supr-con].

- [26] Y. Oreg, G. Refael, and F. von Oppen, *Physical Review Letters* **105**, 177002 (2010), [arXiv:1003.1145 \[cond-mat.mes-hall\]](#).
- [27] V. Mourik, K. Zuo, S. M. Frolov, S. R. Plissard, E. P. A. M. Bakkers, and L. P. Kouwenhoven, *Science* **336**, 1003 (2012), [arXiv:1204.2792 \[cond-mat.mes-hall\]](#).
- [28] S. Nadj-Perge, I. K. Drozdov, J. Li, H. Chen, S. Jeon, J. Seo, A. H. MacDonald, B. A. Bernevig, and A. Yazdani, *Science* **346**, 602 (2014), [arXiv:1410.0682 \[cond-mat.mes-hall\]](#).
- [29] M. Sato and S. Fujimoto, *Phys. Rev. B* **79**, 094504 (2009), [arXiv:0811.3864 \[cond-mat.supr-con\]](#).
- [30] P. A. Lee, *ArXiv e-prints* (2009), [arXiv:0907.2681 \[cond-mat.str-el\]](#).
- [31] L. Fu and C. L. Kane, *Physical Review Letters* **100**, 096407 (2008), [arXiv:0707.1692 \[cond-mat.mes-hall\]](#).
- [32] J. D. Sau, R. M. Lutchyn, S. Tewari, and S. Das Sarma, *Physical Review Letters* **104**, 040502 (2010), [arXiv:0907.2239 \[cond-mat.str-el\]](#).
- [33] This was previously discussed in the dual language of destroying the emerging \mathbb{Z}_2 symmetry in an Ising time crystal in, e.g., Ref. [80].
- [34] R. W. Bomantara and J. Gong, *Phys. Rev. Lett.* **120**, 230405 (2018).
- [35] Raditya Weda Bomantara and Jiangbin Gong, Preprint (2018), [arXiv:1807.07276](#).
- [36] D. E. Liu, A. Levchenko, and H. U. Baranger, *Phys. Rev. Lett.* **111**, 047002 (2013).
- [37] For a protocol that relies on fine-tuning of the Hamiltonian, see Ref. [81].
- [38] J. Alicea, Y. Oreg, G. Refael, F. von Oppen, and M. P. A. Fisher, *Nature Physics* **7**, 412 (2011).
- [39] B. van Heck, A. R. Akhmerov, F. Hassler, M. Burrello, and C. W. J. Beenakker, *New Journal of Physics* **14**, 035019 (2012).
- [40] T. Hyart, B. van Heck, I. C. Fulga, M. Burrello, A. R. Akhmerov, and C. W. J. Beenakker, *Phys. Rev. B* **88**, 035121 (2013).
- [41] D. Aasen, M. Hell, R. V. Mishmash, A. Higginbotham, J. Danon, M. Leijnse, T. S. Jespersen, J. A. Folk, C. M. Marcus, K. Flensberg, and J. Alicea, *Phys. Rev. X* **6**, 031016 (2016).
- [42] T. Karzig, Y. Oreg, G. Refael, and M. H. Freedman, *Phys. Rev. X* **6**, 031019 (2016).
- [43] P. Bonderson, M. Freedman, and C. Nayak, *Phys. Rev. Lett.* **101**, 010501 (2008).
- [44] S. Plugge, A. Rasmussen, R. Egger, and K. Flensberg, *New J. Phys.* **19**, 012001 (2017), [arXiv:1609.01697](#).
- [45] T. Karzig, C. Knapp, R. M. Lutchyn, P. Bonderson, M. B. Hastings, C. Nayak, J. Alicea, K. Flensberg, S. Plugge, Y. Oreg, C. M. Marcus, and M. H. Freedman, *Phys. Rev. B* **95**, 235305 (2017).
- [46] H. Breuer and M. Holthaus, *Physics Letters A* **140**, 507 (1989).
- [47] T. Kitagawa, T. Oka, A. Brataas, L. Fu, and E. Demler, *Phys. Rev. B* **84**, 235108 (2011).
- [48] P. Weinberg, M. Bukov, L. D'Alessio, A. Polkovnikov, S. Vajna, and M. Kolodrubetz, *Physics Reports* **688**, 1 (2017).
- [49] For an overview, see the Supplemental Material as well as Refs. [61, 82, 83].
- [50] T. Karzig, G. Refael, and F. von Oppen, *Phys. Rev. X* **3**, 041017 (2013), [arXiv:1305.3626](#).
- [51] M. S. Scheurer and A. Shnirman, *Phys. Rev. B* **88**, 064515 (2013), [arXiv:1305.4923](#).
- [52] C. S. Amorim, K. Ebihara, A. Yamakage, Y. Tanaka, and M. Sato, *Phys. Rev. B* **91**, 174305 (2015), [arXiv:1405.5153](#).
- [53] T. Karzig, A. Rahmani, F. von Oppen, and G. Refael, *Phys. Rev. B* **91**, 201404 (2015), [arXiv:1412.5603](#).
- [54] T. Karzig, F. Pientka, G. Refael, and F. von Oppen, *Phys. Rev. B* **91**, 201102 (2015), [arXiv:1501.02811](#).
- [55] F. L. Pedrocchi and D. P. DiVincenzo, *Phys. Rev. Lett.* **115**, 120402 (2015), [arXiv:1505.03712](#).
- [56] F. L. Pedrocchi, N. E. Bonesteel, and D. P. DiVincenzo, *Phys. Rev. B* **92**, 115441 (2015), [arXiv:1507.00892](#).
- [57] C. Knapp, M. Zaletel, D. E. Liu, M. Cheng, P. Bonderson, and C. Nayak, *Phys. Rev. X* **6**, 041003 (2016).
- [58] M. Hell, J. Danon, K. Flensberg, and M. Leijnse, *Phys. Rev. B* **94**, 035424 (2016), [arXiv:1601.07369](#).
- [59] M. Sekania, S. Plugge, M. Greiter, R. Thomale, and P. Schmitteckert, *Phys. Rev. B* **96**, 094307 (2017), [arXiv:1703.03360](#).
- [60] A. Rahmani, B. Seradjeh, and M. Franz, *Phys. Rev. B* **96**, 075158 (2017), [arXiv:1605.03611](#).
- [61] B. Bauer, T. Karzig, R. V. Mishmash, A. E. Antipov, and J. Alicea, *ArXiv180305451 Cond-Mat* (2018), [arXiv:1803.05451 \[cond-mat\]](#).
- [62] J. D. Sau and S. D. Sarma, *Nat. Commun.* **3**, 964 (2012).
- [63] I. C. Fulga, A. Haim, A. R. Akhmerov, and Y. Oreg, *New J. Phys.* **15**, 045020 (2013).
- [64] Z. Su, A. B. Tacla, M. Hocevar, D. Car, S. R. Plissard, E. P. A. M. Bakkers, A. J. Daley, D. Pekker, and S. M. Frolov, *Nat. Commun.* **8**, 585 (2017).
- [65] Y. Peng and G. Refael, *ArXiv e-prints* (2018), [arXiv:1805.01896 \[cond-mat.mes-hall\]](#).
- [66] L. D'Alessio and M. Rigol, *Phys. Rev. X* **4**, 041048 (2014), [arXiv:1402.5141](#).
- [67] A. Lazarides, A. Das, and R. Moessner, *Phys. Rev. E* **90**, 012110 (2014), [arXiv:1403.2946](#).
- [68] P. Ponte, A. Chandran, Z. Papić, and D. A. Abanin, *Ann. Phys.* **353**, 196 (2015), [arXiv:1403.6480 \[cond-mat.dis-nn\]](#).
- [69] D. A. Abanin, W. D. Roeck, and F. Huveneers, *Ann. Phys.* **372**, 1 (2016), [arXiv:1412.4752](#).
- [70] P. Ponte, Z. Papić, F. Huveneers, and D. A. Abanin, *Phys. Rev. Lett.* **114**, 140401 (2015), [arXiv:1410.8518 \[cond-mat.dis-nn\]](#).
- [71] A. Lazarides, A. Das, and R. Moessner, *Phys. Rev. Lett.* **115**, 030402 (2015), [arXiv:1410.3455 \[cond-mat.stat-mech\]](#).
- [72] D. A. Abanin, W. De Roeck, and F. Huveneers, *Phys. Rev. Lett.* **115**, 256803 (2015), [arXiv:1507.01474](#).
- [73] D. A. Abanin, W. De Roeck, and W. W. Ho, *Phys. Rev. B* **95**, 014112 (2017), [arXiv:1510.03405](#).
- [74] D. Abanin, W. De Roeck, F. Huveneers, and W. W. Ho, "A rigorous theory of many-body prethermalization for periodically driven and closed quantum systems," (2015), [arXiv:1509.05386](#).
- [75] T. Kuwahara, T. Mori, and K. Saito, *Ann. Phys.* **367**, 96 (2016), [arXiv:1508.05797](#).
- [76] T. Mori, T. Kuwahara, and K. Saito, *Physical Review Letters* **116**, 120401 (2016), [arXiv:1509.03968](#).
- [77] M. Bukov, S. Gopalakrishnan, M. Knap, and E. Demler, *Phys. Rev. Lett.* **115**, 205301 (2015).
- [78] E. Canovi, M. Kollar, and M. Eckstein, *Phys. Rev. E* **93**, 012130 (2016).
- [79] M. Bukov, M. Heyl, D. A. Huse, and A. Polkovnikov,

- [Phys. Rev. B **93**, 155132 \(2016\)](#).
- [80] D. V. Else, B. Bauer, and C. Nayak, [Phys. Rev. X **7**, 011026 \(2017\)](#).
 - [81] C.-K. Chiu, M. M. Vazifeh, and M. Franz, [EPL **110**, 10001 \(2015\)](#).
 - [82] M. Wimmer, [ACM Transactions on Mathematical Software \(TOMS\) **38**, 30 \(2012\)](#).
 - [83] S. Bravyi and D. Gosset, [Commun. Math. Phys. **356**, 451 \(2017\)](#), [arXiv:1609.00735](#).
 - [84] A. Auerbach, *Interacting Electrons and Quantum Magnetism* (1994).

SUPPLEMENTAL MATERIAL

The sweet spots

In this section we revisit the ‘sweet spots’ mentioned in the main text. The ‘sweet spots’ describe locations in the phase diagram where both MZM and MPM are localized on one or two sites, i.e. the correlation length vanishes. Let us provide a simple analytical approach to deriving these sweet spots. First, let us denote each Dirac Fermion operator c by two Majorana operators a and b on each site. Formally we substitute $2c_n = a_n + ib_n$ with $\{a_n, b_m\} = 0$ for all n and m and $a_n^2 = b_n^2 = 1$. (These are related to $\tilde{\gamma}$ introduced in the main text by $a_n = \gamma_{2n-1}$, $b_n = \gamma_{2n}$.) Then the model becomes

$$H_0 = -i\frac{\pi}{T}\lambda_0 \sum_{n=1}^{N-1} a_{n+1}b_n \quad H_1 = -i\frac{\pi}{T}\lambda_1 \sum_{n=1}^N a_n b_n, \quad (9)$$

This model is depicted in Fig. 5.

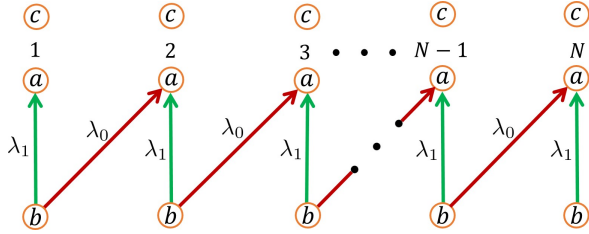


FIG. 5. The Hamiltonian Eq. (9). Red links represent H_0 , and green links H_1 . An application of $U_0 \equiv e^{-iH_0 T/2}$ with $\lambda_0 = 1/2$ exchanges the positions of the MZM b_n and a_{n+1} yielding $b_n \rightarrow a_{n+1}$ and $a_{n+1} \rightarrow -b_n$. Similarly, $U_1 \equiv e^{-iH_1 T/2}$ with $\lambda_1 = 1/2$ carries out the transformation $a_n \rightarrow b_n$ and $b_n \rightarrow -a_n$. The four sweet spots (indicated by crosses in the left panel of Fig. 1 of the main text) are obtained by successive application of U_0 , U_1 and the identity operator (i.e., a vanishing Hamiltonian for time $T/2$) $I = e^{-iH_0 T/2} = e^{-iH_1 T/2}$ with $\lambda_0 = \lambda_1 = 0$. The trivial phase is obtained with the application of IU_1 . The MZM phase, which contain MZM only, is obtained with the application of $U_0 I$. The MPM phase, which has only π modes, is obtained with the application of $U_0 U_1^2$. Finally, the MZM and MPM phase, having both zero and π Majorana modes is obtained with the application of $U_0^2 U_1$. Notice that the application of $U_{0(1)}$ twice is equivalent to taking $e^{-iH_{0(1)} T/2}$ but now with $\lambda_{0(1)} = 1$.

We note that application of $e^{-iH_0 T/2}$ with $\lambda_0 = 1/2$ exchanges the positions of b_n and a_{n+1} for $n = 1, 2, \dots, N-1$. Indeed, defining

$$U_0 \equiv e^{\frac{\pi}{4} \sum_{n=1}^{N-1} b_n a_{n+1}} = \prod_{n=1}^{N-1} B_0^n, \quad B_0^n = e^{\frac{\pi}{4} b_n a_{n+1}}, \quad (10)$$

one can readily check that

$$B_0^{n\dagger} b_n B_0^n = a_{n+1} \quad \text{and} \quad B_0^{n\dagger} a_{n+1} B_0^n = -b_n. \quad (11)$$

Notice that B_0^n and B_0^m commute for $n \neq m$. Similarly

$$U_1 \equiv e^{\frac{\pi}{4} \sum_{n=1}^N a_n b_n} = \prod_{n=1}^N B_1^n, \quad \text{and} \quad B_1^n = e^{\frac{\pi}{4} a_n b_n}, \quad (12)$$

and

$$B_1^{n\dagger} b_n B_1^n = a_n, \quad \text{and} \quad B_1^{n\dagger} a_n B_1^n = -b_n. \quad (13)$$

These operations are depicted in Fig. 5. The arrow indicates which Majorana operator acquires the minus sign. For example, in the application of U_1 (green arrows in Fig. 5), $b_n \rightarrow a_n$ as the arrow directed from b_n to a_n while $a_n \rightarrow -b_n$.

Using these observations, and the identity operator (a vanishing Hamiltonian for $T/2$) $I = e^{-iH_0 T/2} = e^{-iH_1 T/2}$ with $\lambda_0 = \lambda_1 = 0$, it is now straightforward to identified the operation of the Floquet operator $U_F = e^{-iH_0 T/2} e^{-iH_1 T/2}$ at the sweet spots in the various phases.

1. Trivial

The trivial phase is obtained with the application of IU_1 (corresponding to $\lambda_0 = 0, \lambda_1 = 1/2$) then:

$$a_n \xrightarrow{I} a_n \xrightarrow{U_1} -b_n \quad \text{and} \quad b_n \xrightarrow{I} b_n \xrightarrow{U_1} a_n$$

for $n = 1, \dots, N$. So that in the subspace spanned by a_n and b_n the operator $\vec{v}_n \cdot (a_n, b_n)^T$ evolves into $(\bar{U}_F \vec{v}_n) \cdot (a_n, b_n)^T$, with

$$\bar{U}_F = \begin{pmatrix} 0 & 1 \\ -1 & 0 \end{pmatrix} = i\sigma_y,$$

having eigenvalues $\pm i = e^{\pm i\epsilon_n T}$ with quasi-energies $\epsilon_n = \pm\pi/(2T)$ for all n , which are not corresponding to Majorana modes, occurring at quasi-energies zero or π/T .

2. MZM

The phase with MZM only at the two ends of the wire is obtained with the application of $U_0 I$ (corresponding to $\lambda_0 = 1/2, \lambda_1 = 0$) then:

$$a_{n+1} \xrightarrow{U_0} -b_n \xrightarrow{I} -b_n \quad \text{and} \quad b_n \xrightarrow{U_0} a_{n+1} \xrightarrow{I} a_{n+1},$$

for $n = 1, \dots, N-1$. So that in the subspace spanned by a_{n+1} and b_n (for $n = 1, \dots, N-1$) we find, similarly to the trivial case, quasi-energies $\pm\pi/(2T)$, but the Majorana operators a_1 and b_N remain unchanged, establishing the presence of two MZM modes which are localized on one site. In the subspace spanned by a_1 and b_N we find that \bar{U}_F is the identity matrix with eigenvalues $1 = e^{i\epsilon T}$, and two quasi-energies $\epsilon = 0$.

3. MPM

The phase with MPM only at the two ends of the wire is obtained with the application of $U_0 U_1^2$ corresponding to $\lambda_0 = 1/2, \lambda_1 = 1$; notice that the application of $U_{0(1)}$ twice is equivalent to taking $e^{-iH_{0(1)}T/2}$ with $\lambda_{0(1)} = 1$, and results in the multiplication of the Majorana operator by -1 . Then,

$$a_{n+1} \xrightarrow{U_0} -b_n \xrightarrow{(U_1)^2} b_n, \text{ and} \\ b_n \xrightarrow{U_0} a_{n+1} \xrightarrow{(U_1)^2} -a_{n+1},$$

for $n = 1, \dots, N-1$. So that in the subspace of a_{n+1} and b_n (for $n = 1, \dots, N-1$) we find $\bar{U}_F = -i\sigma_y$, and similarly to the trivial case the corresponding quasi-energies $\pm\pi/(2T)$. The Majorana operators a_1 and b_N are special:

$$a_1 \xrightarrow{U_0} a_1 \xrightarrow{(U_1)^2} -a_1 \text{ and} \\ b_N \xrightarrow{U_0} b_N \xrightarrow{(U_1)^2} -b_N.$$

In the subspace of a_1 and b_N we find that \bar{U}_F is equal to the negative of the identity matrix whose two eigenvalues are $-1 = e^{i\epsilon T}$, and two quasi-energies $\epsilon = \pi/T$. This corresponds to MPMS localized at the first and last site of the system.

4. MZM and MPM

The phase with MZM and MPM at the two ends of the wire is obtained with the application of $U_0^2 U_1$ (corresponding to $\lambda_0 = 1, \lambda_1 = 1/2$.) then:

$$a_n \xrightarrow{(U_0)^2} -a_n \xrightarrow{U_1} b_n \text{ and} \\ b_n \xrightarrow{(U_0)^2} -b_n \xrightarrow{U_1} -a_n,$$

for $n = 2, \dots, N-2$. In the subspace of a_n and b_n we find $\bar{U}_F = i\sigma_y$ with quasi-energies $\pm\pi/(2T)$. The Majorana operators a_1, b_1 and a_N, b_N are special:

$$a_1 \xrightarrow{(U_0)^2} a_1 \xrightarrow{U_1} -b_1, \\ b_1 \xrightarrow{(U_0)^2} -b_1 \xrightarrow{U_1} -a_1, \\ a_N \xrightarrow{(U_0)^2} -a_N \xrightarrow{U_1} b_N, \text{ and} \\ b_N \xrightarrow{(U_0)^2} b_N \xrightarrow{U_1} a_N.$$

In the subspace of a_1 and b_1 we find that $\bar{U}_F = -\sigma_x$ with eigenvalues $\mp 1 = e^{i\epsilon T}$, and two quasi-energies $\epsilon = \pi/T$ and $\epsilon = 0$. The corresponding eigen-operators are $(a_1 + b_1)/\sqrt{2}$ and $(a_1 - b_1)/\sqrt{2}$, respectively. Similarly, in the subspace of a_N and b_N we find that $\bar{U}_F = \sigma_x$ with eigenvalues $\pm 1 = e^{i\epsilon T}$, and two quasi-energies $\epsilon = 0$ and $\epsilon = \pi/T$, and the corresponding eigen-operators are $(a_N + b_N)/\sqrt{2}$ and $(a_N - b_N)/\sqrt{2}$, respectively. We therefore find Majorana zero and π modes as symmetric and

anti-symmetric superpositions of the elementary Majorana operators at the first and last sites of the system.

Electrostatic driving

The model described in the main manuscript assumes that all parameters of the Hamiltonian can be controlled in a time-dependent fashion. However, in more realistic situations, one would like to have to control fewer parameters. A particularly attractive scenario is to leave the pairing and the hopping time independent and vary only the on-site potential μ on each site, which in many potential realizations of p -wave superconductors is easily done. For example, in solid-state realizations, one can imagine driving the gates controlling the electrostatic environment. A more direct realization of the Kitaev chain can be implemented by a chain of superconducting quantum dots [62–64], where the potential can be tuned locally for each dot. As we show below, from a theoretical point of view tuning only the chemical potential is equally viable as the model described in the main manuscript, except that such a model does not exhibit the "sweet spot" parameters with zero correlation length for the MZMs and MPMS.

In this section we study a Floquet model in which the Kitaev Hamiltonian is applied over a period T where the chemical potential μ is varied from a value of μ_1 in one part of the cycle to a value μ_2 in the remaining part. The Floquet operator reads:

$$U = e^{-iH_1 T_1} e^{-iH_2 T_2} \quad (14)$$

$$H_j = \sum_i \left[-\mu_j c_i^\dagger c_i - \frac{w}{2} \left(c_i^\dagger c_{i+1} + \text{h.c.} \right) \right. \\ \left. + \frac{\Delta}{2} (c_i c_{i+1} + \text{h.c.}) \right], \quad (15)$$

where the total Floquet period is $T = T_1 + T_2$. One can find the topological invariants of the above system by considering a ring with periodic boundary conditions and noting that at the time-reversal invariant momentum points $k = 0, \pi$ the two parts of the Floquet operator commute since the order parameter vanishes. At these points the quasi-energy is simply the time averaged kinetic energy shifted into the first Floquet zone. This allows us to simplify the general formula of Ref. 1 and write:

$$Q_0 = (-1)^{[\overline{E_k(k=0)T}] + [\overline{E_k(k=\pi)T}]} \\ = (-1)^{[(-\mu_1+w)\lambda T + (-\mu_2+w)(1-\lambda)T]} \\ \times (-1)^{[(-\mu_1-w)\lambda T + (-\mu_2-w)(1-\lambda)T]} \quad (16)$$

$$Q_0 \cdot Q_\pi = (-1)^{[\overline{E_k(k=0)2T}] + [\overline{E_k(k=\pi)2T}]} \\ = (-1)^{[(-\mu_1+w)\lambda 2T + (-\mu_2+w)(1-\lambda)2T]} \\ \times (-1)^{[(-\mu_1-w)\lambda 2T + (-\mu_2-w)(1-\lambda)2T]}. \quad (17)$$

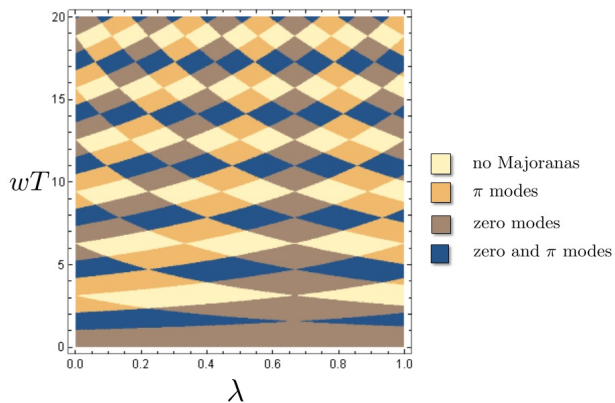


FIG. 6. The phase diagram of the stroboscopic Kitaev model when only the chemical potential μ varies between two values, $\mu_1 = -0.5w$ and $\mu_2 = w$. Both the total time T and the relative first part of the period $\lambda = T_1/T$ are varied.

Here, $\overline{E_k(k)} = \frac{1}{T} \int_0^T (\epsilon_k(t) - \mu(t)) dt$ is the kinetic energy averaged over a period T and we defined the function $[x] = \text{floor}(x/2\pi)$ that counts the number of times the band was folded back into the Floquet zone. It can be checked that Q_0 yields $-(+)$ 1 when zero energy is intersected by an odd(even) number of bands of the kinetic energy $\overline{E_k(k)}$ folded back into the first Floquet zone. Therefore, $Q_0 = -1$ corresponds to the topological phase with MZMs. In Eq. (17) we consider doubling the period which folds back the MPMs to zero energy. The quantity $Q_0 Q_\pi$ then counts the combined parity of pairs of MZMs and MPMs. Note that the first line in each invariant is more general than our stroboscopic model and can be applied to any time dependent Kitaev Hamiltonian. In addition to the stroboscopic time dependence of Eq. (14), we also consider time dependent systems where the chemical potential is of the form $\mu(t) = \mu_0 + \mu_c \cos(\Omega t)$.

Fig. 6 shows the phase diagram of the stroboscopic model when the total period T is varied as well as the relative length of the first part of the period, $\lambda = T_1/T$.

While Eqs. (16),(17) give us the topological invariants they do not predict the size of the gap which is important for the accuracy of our procedure. We therefore look at the stroboscopic model with an example of parameter choice where $T_1 = T_2 = T/2$, $\mu_1 = 2/T$ and varying μ_2 . This gives us all three phases needed for our exchange procedure while the fourth one (a trivial phase) can be achieved by making $\mu_1 = \mu_2 = 2/T$ such that the system is at the trivial equilibrium phase. Fig. 7 shows all quasienergies of a finite chain (of 80 sites) as a function of the changing μ_2 , together with the topological invariants Q_0 and Q_π .

Likewise we model a sinusoidal time dependent chemical potential and arrive at similar results. The quasienergy spectrum is obtained by discretizing time,

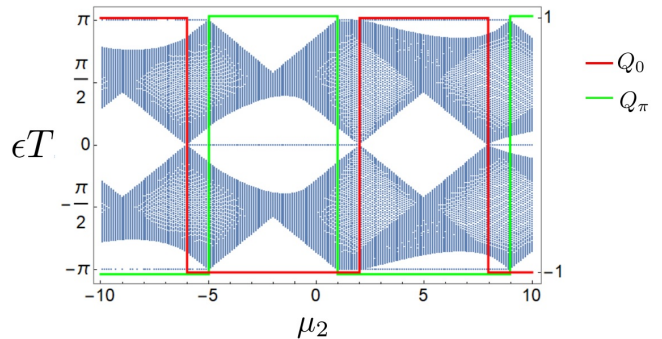


FIG. 7. The quasienergy spectrum of a finite chain in the Floquet-Majorana model (left y-axis) together with the topological invariants (right y-axis). The times T_1 and T_2 are set to 0.45, $\omega = 1$, $\mu_1 = 2$ and μ_2 is scanned.

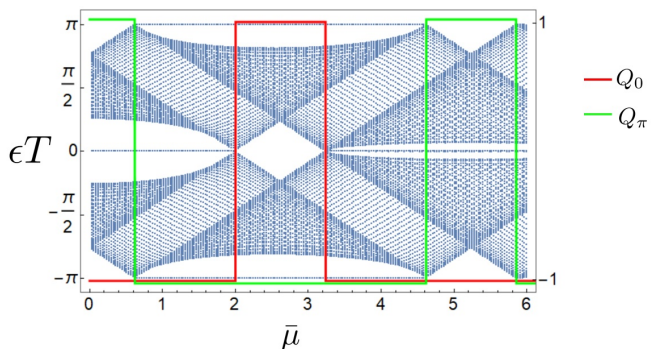


FIG. 8. The quasienergy spectrum of a finite chain in the Floquet-Majorana model (left y-axis) together with the topological invariants (right y-axis). The parameters are $T = 1.2$, $\omega = 1$ and $\mu(t) = \bar{\mu} + \mu_1 \cos(\Omega t)$ with $\mu_1 = 3$.

i.e. calculating the time evolution over a period as the product of evolution operators over small time slices. The results are shown in Fig. 8.

Numerical methods

We now review the method by which we calculate the time evolution of the system. In any time step our Hamiltonian is bilinear in the Majorana operators γ_i and we write its general form as

$$H_{ij}(t) = \vec{\gamma}^T \bar{J} \vec{\gamma} \quad (18)$$

where $\vec{\gamma}$ is a column vector of Majorana operators and \bar{J} is an antisymmetric imaginary matrix. (We denote matrices of c-numbers with an overbar.) The time evolution operator contains an exponent of the Hamiltonian and acts on the Majorana operators. Let us denote by \vec{v}_j the eigenvectors of \bar{J} with corresponding eigenvalues v_j . We can express any linear combination of Majorana

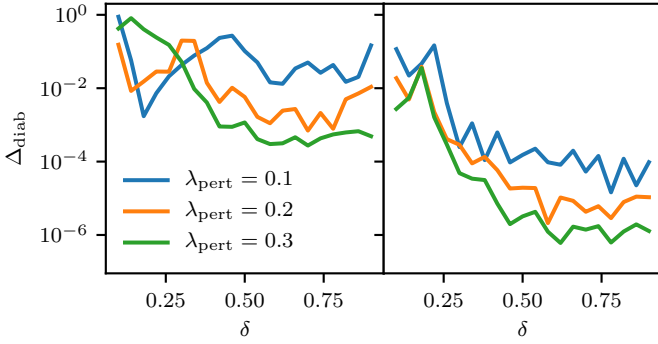


FIG. 9. Diabatic errors for two different values of N_s (left panel: $N_s = 125$, right panel: $N_s = 500$) as a function of δ , the deviation from the critical point, for different strengths of the perturbation used to split the extra pair of MZM and MPM, λ_{pert} . $\delta = 1$ corresponds to the limit of vanishing correlation length. System size is $L = 120$. It is important to note that δ controls the correlation length and the spectral gap, and therefore also bounds the gap induced by the perturbation. For the system size used here, finite-size corrections are less prevalent than diabatic errors.

operators as $V = \vec{V} \cdot \vec{\gamma} = \sum_j \alpha_j \vec{v}_j \cdot \vec{\gamma}$. The action of the evolution operator

$$U_t = \exp(it\vec{\gamma}^T \vec{J} \vec{\gamma})$$

on V can be written as [84]:

$$U_t V U_t^{-1} = (\vec{U}_t \vec{V}) \cdot \vec{\gamma} \quad (19)$$

$$\vec{U}_t = \exp(4it\vec{J}), \quad (20)$$

Note that the factor of 4 stems from the anticommutation relations of Majorana operators $\{\gamma_i, \gamma_j\} = 2\delta_{ij}$. Given the Hamiltonian in each time step, we exponentiate the matrices $\vec{J}(t)$ for each step and multiply them in

the correct order to obtain the full time evolution operator.

Parametric dependence of the diabatic errors

We numerically find that the parameters that control the diabatic errors – system size L , number of steps in which the modes are moved N_s , de-tuning from the critical point δ and perturbation strength λ_{pert} – can exhibit very complicated interplay. Consider, for example, the position in the phase diagram, which we control through the distance to the critical point, δ . This parameter directly or indirectly affects many physical properties of the system and can thus have a complicated effect on the results. Its primary role is to control the spectral gap of the unperturbed Floquet operator and the correlation length of the system. This correlation length controls the exponent with which the hybridization between pairs of MZMs and pairs of MPMS falls off as the distance between them is increased (see also Fig. 2), and thus exponentially affects the splitting. At the same time, since it sets the gap of the undriven Floquet operator, which also bounds the local splitting between MZMs and MPMS that the perturbation can incur, it controls diabatic corrections.

We highlight some of this complicated interplay in Fig. 9. We observe that for small N_s (left panel), the error is largely independent of δ , i.e. how close the system is to the fixed point of vanishing correlation length (which corresponds to $\delta = 1$). For larger N_s , the error decreases as δ is increased, i.e. the system is tuned closer to the "sweet spot". However, in this regime we find that the dependence on system size is very weak (not shown). We conclude from this that the finite-size errors, in particular coming from hybridization between the MZMs and MPMS, are small compared to diabatic errors. The diabatic errors are controlled by the interplay of N_s and the minimal relevant gap, which depending on the parameters can be either the bulk gap (controlled by δ) or the gap induced between MZMs and MPMS in the perturbed region, which depends on both δ and λ_{pert} .